Journal Pre-proof

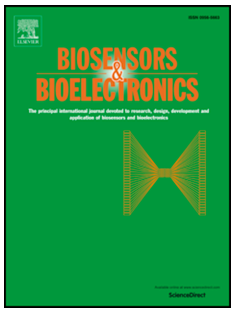

Advances and prospects on acid phosphatase biosensor

Yangxia Han, Kaijun Quan, Jia Chen, Hongdeng Qiu

PII: S0956-5663(20)30660-6

DOI: https://doi.org/10.1016/j.bios.2020.112671

Reference: BIOS 112671

To appear in: *Biosensors and Bioelectronics*

Received Date: 30 June 2020

Revised Date: 21 September 2020

Accepted Date: 30 September 2020

Please cite this article as: Han, Y., Quan, K., Chen, J., Qiu, H., Advances and prospects on acid phosphatase biosensor, *Biosensors and Bioelectronics* (2020), doi: https://doi.org/10.1016/j.bios.2020.112671.

Advances and prospects on acid phosphatase biosensor

Yangxia Han[a], Kaijun Quan[a], Jia Chen[a], Hongdeng Qiu[a,b,c,] *

[a]CAS Key Laboratory of Chemistry of Northwestern Plant Resources, Key Laboratory for Natural Medicine of Gansu Province, Lanzhou Institute of Chemical Physics, Chinese Academy of Sciences, Lanzhou, 730000, China

[b]University of Chinese Academy of Sciences, Chinese Academy of Sciences, Beijing, 100039, China

[c]College of Chemistry, Zhengzhou University, Zhengzhou, 450001, China

* Corresponding author:

E-mail address: hdqiu@licp.cas.cn (H. Qiu)

Abstract: Acid phosphatase (ACP) is a lysosomal enzyme widely found in animals and plants. Particularly, abnormal ACP levels are often closely related to many diseases of the individual and are therefore widely used as biomarkers in clinical diagnosis. With the rapid development of precision medicine, the improvement or enhancement of the selectivity, sensitivity and broad target sample types of ACP biosensors based on the established methods has become an emerging demand for the treatment of diseases related to ACP levels. Therefore, a large number of ACP detection strategies have been used to improve these problems. In this review, the types and advantages/disadvantages of ACP detection methods were summarized and compared. According to the previous reports, the prospects and development trends of ACP detection were discussed. It was expected to provide some insights and inspiration for future research work.

Keywords: acid phosphatase; biosensors; detection methods; review

1. Introduction

Enzyme is a three-dimensional spherical protein molecule that accelerates the rate of a chemical reaction (Chen et al. 2019b). As a green catalyst, the enzyme itself has not been altered in the process of acting on the "substrate" (Zhang et al. 2016a). Acid phosphatase (ACP) (orthophosphate monohydrolase, EC 3.1.3.2) is a lysosomal enzyme, which is a non-specific enzyme capable of hydrolyzing various phosphate esters (Belfiore et al. 1973). Generally, the molecular weights of different types of ACP are different. ACP in plants and individual prostates belong to the high molecular weight group, while low molecular weight enzymes are presented in mammals (Anand and Srivastava 2012). Under acidic conditions at pH 4-7, ACP could catalyze the hydrolysis of phosphate monoesters (Vincent et al. 1992). Most same type ACPs show purple (also known as purple acid phosphatase) due to charge transfer from tyrosine residues to Fe (III) in the enzyme structure. In addition, natural L(+)-tartrate is called tartrate-resistant acid phosphatases (TRAP) because their inhibitory effect is not obvious. However, the inhibitory effect of some ACPs on tartrate is obvious (Mitić et al. 2006; Veeramani et al. 2009; Veeramani et al. 2005). ACP plays a very important role in the metabolism of animals (Lawrence and Van Etten 1981; Siddiqua et al. 2008), plants (Kaida et al. 2008), bacteria and fungi (Leitão et al. 2010; Passariello et al. 2006). Meanwhile, ACP is a scavenger of phosphate (Pi) in plants (Bozzo et al. 2002; Lerner 1999). Pi formed by the hydrolysis of phosphate monoesters by ACP provided a guarantee for the recycling of Pi (Bozzo et al. 2006; Li et al. 2002). In addition, ACP activity could be used as an indicator of soil pH changes (Dick et al. 2000). In mammals, ACP levels are closely related to pathological processes such as primary immune response (Vääräniemi et al. 2004), skeletal remodeling (Ek-Rylander and Andersson 2010), and signaling pathways (Valizadeh et al. 2004). In detail, there are two different types of ACPs in the prostatic tissue, including secreted prostate ACP and cellular ACP, and their isoelectric points and glycosylation are different (Veeramani et al. 2005). Generally, the expression level of an individual's secreted ACP during cancer is higher than that of cellular prostate. Therefore, secreted ACP levels could be considered as prognostic indicators for monitoring prostate cancer treatment (Bozzo et al. 2006; Hassan et al. 2010; Makarov et al. 2009). In addition, serum ACP is considered to be a marker of bone formation and bone resorption in women aged 35-74 years. Generally, high bone resorption rate is closely related to human diseases such as hyperthyroidism, paget's disease, postmenopausal osteoporosis, hyperparathyroidism and

malignant hypercalcemia (Bharathi and Baby 2017; Burstone 1959; Minkin 1982). Moreover, the ACP level in the serum of diabetic patients is elevated (Belfiore et al. 1973). Therefore, it is of great significance to detect ACP changes in plants and animals.

So far, fluorescent, colorimetric, electrochemical, high-performance liquid chromatography (HPLC), surface enhanced Raman scattering (SERS), and Plasmon resonance energy transfer (PRET) methods have been used for the detection of ACP levels (Fredj et al. 2019; Li et al. 2019; Li et al. 2018; Lin et al. 2020; Yamauchi et al. 2005; Yan et al. 2019). The establishment of these methods provided an effective way to detect ACP levels, especially the detection of ACP in body fluids and cells. However, the rapid development of precision medicine is ahead of traditional ACP detection methods. At the same time, in view of the complexity of biological tissues, it is necessary to develop new detection systems to provide services for precision medicine, and provide guarantee for early diagnosis and prognosis monitoring of diseases. Therefore, it is necessary to optimize or integrate existing detection methods or develop new detection methods. More importantly, researching deeply the ACP detection scheme and clinical application based on the existing methods could facilitate the development of human health.

In this paper, we mainly reviewed the current status of ACP detection around fluorescent, colorimetric, electrochemical, and other detection strategy (Fig. 1). Among the above methods, the fluorescence detection method was a widely used, which showed that the fluorescence method was the most popular for detecting ACP because of its simplicity, convenience and speed. At the same time, colorimetric and electrochemical detection also play an irreplaceable role. It was hoped that this review could inspire new strategies for detecting ACP and provide ideas for clinical diagnosis and disease treatment related to ACP levels.

2. Progress of ACP detection strategies

2.1 Fluorescence detection strategy

Fluorescence detection technology has become one of the most important methods of ACP analysis due to its advantages such as high sensitivity, short response time, good selectivity, convenience, fastness and high accuracy (Yi et al. 2009; Zhang et al. 2016b; Zhang et al. 2016c; Zheng et al. 2013). Fluorescence method could directly or indirectly detect the concentration of

ACP through the change of the fluorescence intensity (increase or decrease) of the sensor, which was the most widely used method for detecting ACP. According to the actual detection requirements, "turn-on", "turn-off' and ratiometric modes could be used to obtain the ACP level.

2.1.1 "Turn-on" mode

"Turn-on" mode refers to a detection strategy in which the fluorescent signal of a sensor with potential sensing performance is enhanced or highlighted. "Turn-on" mode was the most widely used mode in the analysis of ACP. Generally, three types of materials such as compounds based on organic molecular structural units, carbon- and metal-based nanomaterial were served in the detection of ACP (Qu et al. 2018; Xie et al. 2012; Xu et al. 2020).

Sensors based on organic molecular structural units were most widely used in the detection of ACP. However, although the design procedure of the sensor was more complicated, the analysis of ACP was still completed. Xie et al. introduced a sensor for ACP and inhibitors sensing based on cationic conjugated polyelectrolyte (PPE4+), which was able to link with p-nitrophenyl phosphate (p-NPP). However, the p-NPP was hydrolyzed to p-nitrophenyl (p-NP) when ACP was added, resulting in the non-fluorescent complex of PPE4+/p-NPP altered to the fluorescent PPE4+. Thus, this sensor successfully achieved the determination of ACP, the limit of detection (LOD) was 0.17 nM (Xie et al. 2012). Immediately after, some sensors were developed to detect ACP activity and screen inhibitors (Dwivedi and Iyer 2013; Guo et al. 2013; Xu et al. 2014). However, in recent years, compounds with small molecules as structural units have not been explored in the detection of ACP. This may be related to the relative lack of advantages of the materials.

Relatively, carbon-based nanomaterial was an environmentally friendly nanomaterial and has attracted wide attentions (Chen et al. 2017). In 2017, a sensor based on nitrogen-doped graphene quantum dots (N-GQDs) to detect tyrosinase (TYR) and ACP was developed. The detection process involved tyrosine catalyzed by TYR to generate dopaquinone, which could quench the fluorescence of N-GQDs. L-ascorbic acid-2-phosphate (AA2P) was hydrolyzed to produce ascorbic acid (AA) in the presence of ACP and dopaquinone was reduced to L-dopa by AA, resulting in the restoration of fluorescence of N-GQDs. Therefore, the sensor realized the detection of ACP with a LOD of 0.014 U/L and the application of actual samples (Qu et al. 2018). Subsequently, they applied glutathione-functionalized graphene quantum dot (GQDs@GSH) to establish a method for detecting ACP and screening inhibitor parathion-methyl (Qu et al. 2019). Similarly, Zhu et al.

described a fluorescence method for detecting ACP based on nitrogen-doped carbon dots (N-CDs) (Zhu et al. 2018). A carbon dots (CDs) sensor that detected Cu^{2+} and ACP was fabricated. The fluorescence of CDs was quenched by Cu^{2+} would be restored again by adding of AA. Therefore, the sensor achieved ACP sensing with a LOD of 60 μM by utilizing the property that AA2P was hydrolyzed by ACP to AA (Ma et al. 2019).

In recent years, although metal-based nanomaterials did not shared the bio-friendliness of carbon-based nanomaterials, they have still attracted considerable attentions. Liu et al. introduced L-cysteine-modified $CuInS_2$ QDs (L-cys-$CuInS_2$ QDs) sensor for ACP detecting. The addition of $(NaPO_3)_6$ could quench the fluorescence of L-cys-$CuInS_2$ QDs, which would be restored due to the hydrolysis of $(NaPO_3)_6$ by ACP (Fig. 2). Therefore, the sensor could be used for the evaluation of ACP level with a LOD was 9.02 μU/L and the analysis of actual samples (Liu et al. 2015). In 2017, a lysozyme-stabilized near-infrared fluorescent gold/silver nanocluster (Lys-Au/AgNCs) was used to detect ACP. The AA formed by the hydrolysis of AA2P by ACP could significantly enhance the fluorescence signal of Lys-Au/AgNCs. Therefore, a "turn-on" mode detection method was developed for ACP (Pang and Liu 2017). Recently, Xu et al. established a dual-mode AuNCs/MnO_2 nanocomposite sensor for ACP sensing. The linear ranges of the colorimetric and the fluorescent method were 0.05-16 U/L and 0.01-16 U/L, respectively. The LOD were 0.017 U/L and 0.003 U/L (Xu et al. 2020). Importantly, AuNCs/MnO_2 sensor could monitor the dynamic changed of ACP during soil cadmium pollution, which was different from previous biological sample detection applications. It was expected to provide design ideas for monitoring the dynamic changed of ACP during the pathological process of organisms.

2.1.2 "Turn-off" mode

"Turn-off" mode, as a quenching detection process, did not display the advantages of "turn-on" mode such as high sensitivity and avoiding the occurrence of error signals (Han et al. 2019). However, when the sensor of "turn-on" mode could not meet the detection requirements, the "turn-off" mode could become a supplementary solution. Generally, the sensors that detect ACP in "turn-off" mode were based on carbon nanomaterials, metal nanoclusters and quantum dots (Huang et al. 2016; Qian et al. 2015; Wang et al. 2016).

Carbon nanomaterials were widely used for ACP detection due to their excellent performances such as low toxicity, biological compatibility, resistance to photobleaching (Duan et al. 2015;

Strauss et al. 2014; Wu et al. 2015). Qian et al. constructed a method for reversibly detecting ACP and screening inhibitors based on carbon quantum dot (CQD) sensor. The fluorescence of Ni^{2+}-regulated CQD would be restored by the introduction of pyrophosphate (PPi) due to the binding force between Ni^{2+} and -COOH was stronger than that of PPi. Interestingly, ACP could hydrolyze PPi, causing free Ni^{2+} to bind to -COOH on the surface of CQD again, further leading to CQD aggregation and fluorescence quenching (Fig. 3). The established method realized the detection of ACP in the range of 18.2-1300 U/L, and the LOD was 5.5 U/L (Qian et al. 2015). The advantage of this method was that CQD sensors could be reused, which was a method of saving resources. Similarly, the GQDs based on redox reactions to detect AA and ACP was designed. In detail, Cr^{3+} was prone to electrostatic adsorption with -COOH and -OH on the surface of GQDs, causing the fluorescence of GQDs to be quenched. In addition, AA could reduce $Cr_2O_7^{2-}$ to Cr^{3+}. Therefore, AA produced by ACP hydrolysis AA2P could be used to reduce $Cr_2O_7^{2-}$ to Cr^{3+}, so as to achieve the determination of AA and ACP. The LODs of GQDs sensor for AA and ACP were 0.28 μM and 8.9 mU/L, respectively. The actual sample analysis data verified the excellent performance of the sensor (Shi et al. 2016). Subsequently, Na et al. established a GQD sensor for detecting ACP using poly- (dimethyl diallyl ammonium chloride) (PDDA) and $(NaPO_3)_6$ as intermediates (Na et al. 2016a). In 2019, Chen et al. conducted dopamine under the addition of ACP to form polydopamine, which could generate internal filtering effect mechanism with fluorescent CDs. Thus, a new method for detecting ACP was constructed based on the quenching of fluorescence of CDs by polydopamine, the LOD was 0.45 U/L (Chen et al. 2019c). The excellent performance of the sensor in serum samples proved that the method has considerable application prospects in the clinical and biomedical fields.

Compared with carbon nanomaterials, metal nanoclusters (NCs) or quantum dots (QDs) have high toxicity and expensive metal prices (Zhong et al. 2020). But they still obtained the extensive attentions due to their excellent photophysical properties, such as high quantum yield, large Stokes shift, and narrow emission bands (Liu et al. 2011; Sharma et al. 2012; Zhang et al. 2012). Sun et al. synthesized AuNCs@GSH/MUA with glutathione (GSH) and 11-mercap toundecanoic acid (MUA) as functional ligands and used for ACP detection and inhibitor screening. The addition of Fe^{3+} would cause the fluorescence of AuNCs@GSH/MUA to be quenched. However, the fluorescence of AuNCs@GSH/MUA-Fe^{3+} was restored again when PPi was introduced. Subsequently, free Fe^{3+}

could induce the fluorescence of AuNCs@GSH/MUA to be quenched after PPi was hydrolyzed by ACP. Based on changed in the fluorescence signals, the linear range and LOD of the sensor for ACP were 1-30 nM and 1 nM, respectively (Sun et al. 2015). Huang et al. applied a competitive hydrophobic interaction between p-NP and α-cyclodextrin to construct a CuNCs sensor that reversibly detected ACP. The surface hydrophobicity of fluorescent CuNCs aggregates made it possible to adsorb p-NP, resulting in fluorescence being quenched. However, the strong host-guest interaction between α-cyclodextrin and p-NP would cause p-NP to detach from the surface of CuNCs, resulting in fluorescence being appeared. Therefore, they used the property that p-NPP could be hydrolyzed by ACP to p-NP to realize the detection of ACP in the linear range of 3.8-22.8 U/L, and the LOD was 1.3 U/L. The application of the sensor in human serum and seminal plasma also proved the feasibility of the method (Huang et al. 2016). Subsequently, they fabricated CuNCs sensor for reversible ACP detection using Fe^{3+} and PPi as intermediates (Zhao et al. 2017). In addition, a near-infrared $CuInS_2$ quantum dot (QD) coated with mercaptopropionic acid (MPA) was introduced for ACP sensing. The addition of Cu^{2+} could quench the fluorescence of the probe. Subsequent addition of ATP, which has a strong interaction with Cu^{2+}, could cause the fluorescence recovery of $CuInS_2$ QDs. However, ACP could catalyze the hydrolysis of ATP, causing the Cu^{2+}-ATP complex to be disassembled. Therefore, the recovered fluorescence was quenched again by ACP adding. Near-infrared $CuInS_2$ QDs-based probes successfully imaged human prostate cancer cells in vitro (Lin et al. 2015). This sensor was the most sensitive sensor for ACP in “turn-off” mode so far. Wang et al. capped CdTe QDs with cysteamine, $-NH_2$ on the surface of CdTe QDs could form electrostatic and hydrogen bonding with ATP when ATP was added, resulting in enhanced fluorescence of CdTe QDs. The addition of ACP could hydrolyze ATP, leading to the attenuation of CdTe QDs fluorescence. The linear range and LOD of the sensor to ACP were 1.0-50 mU/L and 0.45 mU/L, respectively. The established method also realized screening and detection of parathion-methyl (Wang et al. 2016).

2.1.3 Ratiometric mode

The development of the ratiometric mode sensor was later than the “turn-on” and “turn-off” modes for the determination of ACP. However, ratiometric mode was a method worthy of promotion because of its strong anti-interference ability (Han et al. 2020; Li et al. 2020; Song et al. 2017). Generally, when a target was added to a dual-wavelength sensor, the fluorescence intensity at

these two wavelengths would increase and/or decrease. According to the change of the fluorescence intensity ratio, the analysis of the target could be realized successfully.

Based on the above phenomenon, Na et al. combined Nile red (NR) with GQD via a lecithin/β-cyclodextrin (lecithin/β-CD) complex as a linker to fabricate ratiometric method based on Förster resonance energy transfer (FRET) mechanism. The introduction of energy acceptor NR could weaken the fluorescence of energy donor GQDs and enhance the fluorescence of NR. However, the presence of ACP would decompose lecithin and cause NR to escape from GQDs. This procedure inhibited the FRET process, resulting in enhanced fluorescence of GODs and decreased fluorescence of NR, which could achieve in vitro imaging of human prostate cancer cells. The linear range and LOD of this method for ACP were 0-1500 mU/L and 28 mU/L, respectively (Na et al. 2016b). A metal organic framework (MOF)-based NH_2-MIL-101 MOF biosensor that emitted fluorescence at 456 nm was designed. As a peroxide nanozyme, NH_2-MIL-101 MOF could oxidize o-phenylenediamine (OPD) to 2,3-diaminophenazine with a maximum emission wavelength of 556 nm in the presence of H_2O_2, resulting in attenuation of fluorescence at 456 nm. When PPi was added to the NH_2-MIL-101/OPD/H_2O_2 system, PPi could specifically bind to the Fe center in NH_2-MIL-101 MOF. Therefore, the activity and inherent fluorescent properties of the nanoenzyme were inhibited and retained, respectively. However, PPi would be hydrolyzed by ACP and the fluorescence of 2,3-diaminophenazine at 556 nm would be enhanced when PPi and ACP were introduced to the above system (Fig. 4). The linear range and LOD of the described sensor were 0.01-30 U/L and 0.005 U/L, respectively. To verify the practicability of the method, the obtained sensor has been successfully used for the analysis of ACP in serum samples (Li et al. 2019). Subsequently, the double-emitting nitrogen-doped carbon dots (N-CDs) at 415 and 509 nm was prepared by hydrothermal method. In detail, $(NaPO_3)_6$ could cause aggregation-induced quenching of fluorescence of positively charged N-CDs at 509 nm. Interestingly, the hydrolysis of $(NaPO_3)_6$ by ACP induced the fluorescence of N-CDs to be restored again. Therefore, a method based on N-CDs for detecting ACP, screening inhibitors and determining ACP in HePG2 cells was successfully constructed (Zhu et al. 2019). Similarly, the two-emission carbon dots (GN-CDs) were synthesized by hydrothermal method and realized the detection of Fe^{3+} and ACP. However, the GN-CDs were only used for the detection of ACP in water samples and were not screened for inhibitors, which did not give full play to the excellent performance of GN-CDs (Pang and Liu 2020). Therefore, for the

ratiometric mode detection, only by applying the sensor to the detection of ACP in vitro and vivo, the advantages of the sensor to avoid the interference of autofluorescence of the organism could be highlighted. Notably, a comparison of detection performance for ACP based on the different fluorescent detection modes has been provided in Table 1.

2.2 Colorimetric detection strategy

Colorimetry, as a method of quantitative analysis, was a method of obtaining the content of a component by comparing or measuring the color depth of a colored substance solution. The basis of this method was the chromogenic reaction of the compounds. Commonly, there were two colorimetry in the early days, namely visual colorimetry and photoelectric colorimetry, both of which were based on Lambert-Beer law ($A=\varepsilon bc$). Generally, the visual colorimetric method was the standard series method, the standard solution with different content of the analyte in the same set of colorimetric tubes was first developed according to the analysis steps, and the standard color scale with gradually changing color. The sample solution was also developed color under the same conditions and compared with the standard color scale. Subsequently, visually find the standard sample that was closest to the color of the sample to be tested, and calculate the content of the component to be tested. Compared with visual colorimetry, photoelectric colorimetry measured the absorbance of a series of standard solutions on a photoelectric colorimeter and plotted a working curve of absorbance versus concentration, then obtained the content of the component to be measured on the working curve according to the absorbance of the sample. Therefore, the photoelectric colorimetry method could eliminate subjective errors and improve measurement accuracy. Moreover, the filter could be selected to eliminate interference, thereby improving selectivity. However, the photoelectric colorimetric method was replaced by a spectrophotometric method because it could not obtain a monochromatic beam, resulting in the spectrophotometry was mostly used at present (Clydesdale and Ahmed 1978; Ohta and Robertson 2006; Schanda 2007). In the colorimetric detection process, the concentration of ACP was often reflected indirectly through intermediates and substrates.

For the first time, a colorimetric method for detecting ACP and alkaline phosphatase (ALP) was reported. In detail, after adding ACP or ALP to the coexistence system of $Cu(BCDS)_2^{2-}$ (BCDS=bathocuproinedisulfonate) and AA2P, AA converted from AA2P could reduce $Cu(BCDS)_2^{2-}$

to $Cu(BCDS)_2^{3-}$, the charge transfer mechanism was supported by the results of quantum mechanical computations. Therefore, the UV-vis absorption spectrum showed an absorption peak at 484 nm, and the color of the solution changed from colorless to orange-red. The probe could not only detect ACP and ALP in the range of 0-220 U/L, but also verify the presence of ACP and ALP in serum. The LODs were ~3.16 U/L and ~1.27 U/L, respectively (Hu et al. 2016). Deng et al. prepared Ch-PtNPs oxide mimetic enzymes by capping chitosan (Ch) on platinum nanoparticles (PtNPs). The results showed that acidic conditions could significantly shorten the chromogenic reaction time of Ch-PtNPs oxidase to 3,3',5,5'-tetramethyl-benzidine (TMB), but AA could significantly inhibit the activity of Ch-PtNPs oxidase. Therefore, they added ACP to the solution of Ch-PtNPs oxidase, TMB and AA2P, which led to ACP catalyzed AA2P production of AA to inhibit the activity of Ch-PtNPs oxidase, further leading to no change in the color of TMB. The linear range and LOD of ACP for this method were 0.25-2.5 U/L and 0.016 U/L, respectively. Meanwhile, the detection of ACP in biological samples and the screening of ACP inhibitors were achieved (Deng et al. 2017). Subsequently, Guo et al. proposed a method that ACP could hydrolyze PPi to Pi in a chelate formed by Cu^{2+} and PPi. The released Cu^{2+} could induce the activity of C_3N_4 nanosheet mimic enzyme. After the addition of H_2O_2, the system consisted of Cu^{2+} and C_3N_4 nanosheet led to the conversion of TMB to colored oxTMB (Fig. 5A). Based on this phenomenon, a colorimetric detection ACP method was established with a linear range and LOD of 0.05-40 U/L and 8.8 mU/L, respectively (Guo et al. 2019). Subsequently, a method was established to detect ACP based on AuPd nanozymes to regulate the color reaction between H_2O_2 and TMB. AA produced by adding ACP to AA2P induced H_2O_2 into •OH, which made the color reaction of TMB suppressed. The linear range and LOD of this method were 1-14 U/L and 0.53 U/L, respectively (Zheng et al. 2020). Haddada et al. established a platform for sensitive detection of prostate ACP based on biphosphonates-PEG-coated gold nanoparticles (BP-PEG-AuNPs), its color changed from wine red to purple/blue when the concentration of prostate ACP gradually increased. This strategy could achieve prostate ACP detection in the fg range (1 fg/mL-1 mg/mL) with a LOD of 0.3 fg/mL. Importantly, a visual LOD of 1 ng/mL could also be achieved, which allowed the naked eye or image analyzer to quickly detect prostate ACP (Haddada et al. 2017). Compared with ordinary mimic enzymes, oxidative mimic enzymes displayed excellent oxide properties, which made it unnecessary to resort to the destructive H_2O_2 in mediating the oxidation color reaction of TMB.

Therefore, researchers established some colorimetric method for the detection of ACP using PdPt bimetal alloy nanowires (Pd/Pt NWs), Co/Mn oxide nanocomposite and two-dimensional Pd nanoplates enclosed by {100}-facets [{100}PdSP@rGO] oxidase mimics (Fig. 5B), respectively. Currently, oxidase mimics could mediate the oxidation reaction of TMB. However, when ACP was introduced into the substrate AA2P in the above method, the generated AA significantly inhibited the activity of the oxidase mimic. The linear ranges of the above methods were 0.17-2.67 U/L, 0.02-1.0 U/L and 0.01-6.0 U/L, and the LOD were 0.06 U/L, 8.2 mU/L and 8.3 mU/L, respectively (Chen et al. 2019a; Jin et al. 2019; Zhang et al. 2019b). Subsequently, Lin et al. implemented ACP detection using a similar mechanism. Notably, AA, which was produced by ACP hydrolysis of AA2P, could inhibit the color reaction of 2,2'-azino-bis (3-ethylbenzothiazoline-6- sulfonic acid) (ABTS) (Fig. 5C**)**. The linear range and LOD of the method were 0.09-7.3 U/L and 0.011 U/L, respectively (Lin et al. 2020). As can be seen from Table 1, the sensitivity of the ACP colorimetric sensor was usually inferior to that of the fluorescence sensor.

2.3 Electrochemical detection strategy

The application of electrochemical methods was often less than colorimetric and fluorescent methods for ACP sensing. In the process of electrochemical measurement, an intermediate that has an electrochemical response to an electrode modified with a material was needed. The concentration of ACP could be indirectly reflected by monitoring the current or potential in the substrate. The advantages of the electrochemical method were that the instrument used was small, simple, portable, and the detection time was short, which could not be achieved by the colorimetric method (Ben Brahim et al. 2016; Song et al. 2019).

Hassan et al. prepared a novel poly(vinyl chloride) matrix membrane-based electrochemical sensor that responded to p-NPP at a concentration range of 9.6×10^{-6} to 1.0×10^{-2} M showed a near-Nernst response to p-NPP. Under the optimal pH and temperature conditions, the concentration of p-NPP would be altered effectively by ACP and ALP activity. Therefore, the sensor could achieved the detection of ACP and ALP in the range of 50-3000 IU/L and 30-3400 IU/L, and the LOD was 0.03-0.05 enzyme IU/L (IU is the international unit) (Hassan et al. 2009). Similarly, a sensor that detected ACP based on a poly (vinyl chloride) matrix membrane was designed. The concentration of α-naphthoic acid phosphate (1-NAP) with near-Nernst response would be changed

by adding ACP. Based on this phenomenon, the sensor not only achieved the detection of ACP in the range of 0.01-4.3 IU/L, but also detected the activity of ACP in biological fluids of patients with prostate cancer (Kamel et al. 2014). Subsequently, Fredj et al. established a sensor based on 2,9,16,23-tetracarboxylic acid-polyacrylamide [Cu(II) TC Pc-PAA] modified screen-printed gold transducer. In detail, the sensor could detect the phosphate generated by hydrolysis of 2-naphthyl phosphate with ACP, thereby indirectly detecting ACP. The linear range and LOD of the method were 0.5-20 nM and 0.5 nM, respectively (Fredj et al. 2019). Interestingly, Huang et al. designed a 3,5-diamino- 1,2,4 triazole-modulated TNA/g-C_3N_4/DAT sensor, which was penetrated into a solution containing Fe^{3+}, AA2P, and ACP, then AA produced by ACP hydrolysis AA2P could reduce Fe^{3+} to Fe^{2+}. Immediately, the coordination between Fe^{2+} and DAT would result in an increase in photocurrent (Fig. 6). The increase value in photocurrent and ACP showed a good linear relationship in the range of 0.05-100 U/L, with a LOD of 0.016 U/L. The sensor enabled the analysis of ACP in human blood samples (Huang et al. 2020). In addition, a comparison of electrochemical detection performance for ACP based on different materials has been provided in Table 1.

2.4 Other detection strategies

Compared with the fluorescent, colorimetric and electrochemical methods commonly used by researchers, there were still some methods for detecting ACP that were rarely appeared. For example, Yamauchi et al. utilized high performance liquid chromatography with an electrochemical detector (ECD/HPLC) to detect ACP in cathodic mode due to the p-NP produced by the hydrolysis of p-NPP disodium salt by ACP has electrochemical response activity (Yamauchi et al. 2004). Similarly, they subsequently developed a same method for indirect detection of ACP based on p-NPP (Yamauchi et al. 2005). Li et al. introduced a SERS sensor. Preparation of molecularly imprinted polymers (MIPs) that specifically recognized ACP was necessary for this sensor. SERS signals would appear when ACP and AuNPs modified with phenylboronic acid (MPBA) were added to the detection system, due to the stronger affinity between MPBA and ACP. The linear range and LOD of the Raman probe to ACP were 18.2 pM-1.82 μM and 18.2 pM, respectively (Li et al. 2018). Although this was the most sensitive sensor so far, the complicated steps in designing the sensor have severely limited the widespread application of MIPs. Zhang et al. first established a chemical

exchange saturation transfer magnetic resonance imaging contrast agent (PhenolCEST MRI) using an exchangeable hydroxyl proton with a resonance frequency of 4.8 ppm in water contained in ^{1}H nuclear magnetic resonance (^{1}H NMR) spectroscopy. At pH=5, p-NPP was hydrolyzed by ACP to CEST-detectable phenol, which could further quantify ACP in the range of 5-50 U/L. This method also measured ACP activity in prostate cell lysates. However, the detection time of ACP by PhenolCEST MRI was significantly longer than other methods (Zhang et al. 2019a). PRET was a detection principle that occurred between noble metal nanoparticles (donors) and conjugated molecules or nanoparticles (acceptors). Yan et al. used urchin-like gold nanoplasmonics (UGPs) and oxTMB as donors and acceptors to establish a scattering method for detecting ACP. In detail, when oxTMB was introduced in UGP system, PRET would cause resonance quenching in the localized surface Plasmon resonance spectrum. However, when AA2P was hydrolyzed by ACP, the generated AA could reduce oxTMB to TMB, thereby inhibiting the occurrence of PRET (Yan et al. 2019). The corresponding analysis performance of these sensors has been displayed in the Table 1.

3. Conclusion and prospective

This paper reviewed the ACP sensors based on fluorescent, colorimetric, electrochemical and other methods. For testing the performance of ACP, the LOD, substrates and materials used in different strategies were compared. The results showed that the fluorescence strategy was the most widely used method among all detection methods. In addition, almost all methods used substrates when detecting ACP. Among them, AA2P, p-NPP, PPi, and $(NaPO_3)_6$ were commonly used intermediates, and the changed in the fluorescent signal mediated by them could indirectly demonstrate the activity or concentration of ACP. Importantly, only a few red or near-infrared fluorescent materials were used to detect ACP. Therefore, in order to meet the needs of the development of precision medicine, it was urgent to construct some sensors that detect ACP based on long-wave emission fluorescent materials or other materials, because these materials could avoid background fluorescence interference from living organisms or substrates. Secondly, the use of chemical informatics to simulate the spatial force and bond energy between the sensor and ACP/intermediates could provide a theoretical basis for the design of sensors specifically sensing ACP. Finally, according to the structural characteristics and physical/chemical properties of ACP, designing new materials or new methods for detecting ACP was also worth looking forward to by

researchers. In summary, with the continuous development of ACP sensors, a convenient, simple, fast, sensitive and efficient detection method will usher in a research boom, providing a basis for the rapid development of precision medicine.

Declaration of competing interest

The authors declare that they have no known competing financial interests or personal relationships that could have appeared to influence the work reported in this paper.

CRediT authorship contribution statement

Yangxia Han: Writing original draft.

Kaijun Quan: Making suggestions for original draft.

Jia Chen: Making suggestions for original draft.

Hongdeng Qiu: Writing original draft.

Acknowledgments

The authors are grateful for financial support from National Key Research and Development Program (No. 2019YFD1002403) and National Natural Science Foundation of China (No 21822407).

References

Anand, A., Srivastava, P.K., 2012. Appl. Biochem. Biotech. 167(8), 2174-2197.

Askari, F., Rahdar, A., Trant, J.F., 2019. Sens. Bio-Sens. Res. 22, 100251.

Belfiore, F., Napoli, E., Vecchio, L., Rabuazzo, A., 1973. Am. J. Med. Sci. 266(2), 139-143.

Ben Brahim, M., Belhadj Ammar, H., Abdelhédi, R., Samet, Y., 2016. Chin. Chem. Lett. 27(5), 666-672.

Bharathi, R., Baby, D., 2017. Int. J. Chem. Stud. 5(4), 425-429.

Bozzo, G.G., Dunn, E.L., Plaxton, W.C., 2006. Plant, Cell Environ. 29(2), 303-313.

Bozzo, G.G., Raghothama, K.G., Plaxton, W.C., 2002. Eur. J. Biochem. 269(24), 6278-6286.

Burstone, M., 1959. J. Histochem. Cytochem. 7(1), 39-41.

Chen, C., Liu, W., Ni, P., Jiang, Y., Zhang, C., Wang, B., Li, J., Cao, B., Lu, Y., Chen, W., 2019a. ACS Appl. Mater.

Interfaces 11(50), 47564-47570.
Chen, C., Wu, Z., Wang, T., Wan, X., Zhen, S., Huang, C., 2017. Chin. Chem. Lett. 28(7), 1385-1390.
Chen, D., Qin, W., Fang, H., Wang, L., Peng, B., Li, L., Huang, W., 2019b. Chin. Chem. Lett. 30(10), 1738-1744.
Chen, Y., Wang, Z., Hao, X., Li, F., Zheng, Y., Zhang, J., Lin, X., Weng, S., 2019c. Sens. Actuators, B 297, 126784.
Clydesdale, F.M., Ahmed, E., 1978. Crit. Rev. Food Sci. Nutr. 10(3), 243-301.
Deng, H., Lin, X., Liu, Y., Li, K., Zhuang, Q., Peng, H., Liu, A., Xia, X., Chen, W., 2017. Nanoscale 9(29), 10292-10300.
Dick, W.A., Cheng, L., Wang, P., 2000. Soil Biol. Biochem. 32(13), 1915-1919.
Duan, H., Wang, D., Li, Y., 2015. Chem. Soc. Rev. 44(16), 5778-5792.
Dwivedi, A.K., Iyer, P.K., 2013. Anal. Methods 5(9), 2374-2378.
Ek-Rylander, B., Andersson, G., 2010. Exp. Cell Res. 316(3), 443-451.
Fredj, Z., Ali, M.B., Abbas, M.N., Dempsey, E., 2019. Anal. Chim. Acta 1057, 98-105.
Guo, P., Yan, S., Zhou, Y., Wang, C., Xu, X., Weng, X., Zhou, X., 2013. Analyst 138(12), 3365-3367.
Guo, Y., Li, X., Dong, Y., Wang, G., 2019. ACS Sustainable Chem. Eng. 7(8), 7572-7579.
Haddada, M.B., Aouidat, F., Monteil, M., Lecouvey, M., de la Chapelle, M.L., Spadavecchia, J., 2017. Frontiers Lab. Med. 1(4), 186-191.
Han, J., Yue, X., Wang, J., Zhang, Y., Wang, B., Song, X., 2020. Chin. Chem. Lett. doi.org/10.1016/ j.cclet.2020.01.029
Han, Y., Chen, J., Li, Z., Chen, H., Qiu, H., 2019. Biosens. Bioelectron. 111811.
Hassan, M.I., Aijaz, A., Ahmad, F., 2010. Expert Rev. Anticanc. 10(7), 1055-1068.
Hassan, S.S., Sayour, H.E., Kamel, A.H., 2009. Anal. Chim. Acta 640(1-2), 75-81.
Hu, Q., Zhou, B., Li, F., Kong, J., Zhang, X., 2016. Chem. Asian J. 11(21), 3040-3045.
Huang, M., Tian, J., Zhou, C., Bai, P., Lu, J., 2020. Sens. Actuators, B 127654.
Huang, Y., Feng, H., Liu, W., Zhou, Y., Tang, C., Ao, H., Zhao, M., Chen, G., Chen, J., Qian, Z., 2016. Anal. Chem. 88(23), 11575-11583.
Jin, L., Sun, Y., Shi, L., Li, C., Shen, Y., 2019. J. Mater. Chem. B 7(29), 4561-4567.
Kaida, R., Hayashi, T., Kaneko, T.S., 2008. Phytochemistry 69(14), 2546-2551.
Kamel, A.H., Galal, H.R., Hanna, A.A., 2014. Int. J. Electrochem. Sci 9, 5776-5787.
Lawrence, G.L., Van Etten, R.L., 1981. Arch. Biochem. Biophys. 206(1), 122-131.
Leitão, V.O., de Melo Lima, R.C., Vainstein, M.H., Ulhoa, C.J., 2010. Biotechnol. Lett. 32(8), 1083-1088.
Lerner, H.R., 1999. Plant responses to environmental stresses: from phytohormones to genome reorganization.
Li, D., Zhu, H., Liu, K., Liu, X., Leggewie, G., Udvardi, M., Wang, D., 2002. J. Biol. Chem. 277(31), 27772-27781.
Li, S., Hu, X., Chen, Q., Zhang, X., Chai, H., Huang, Y., 2019. Biosens. Bioelectron. 137, 133-139.
Li, X., Li, B., Hong, J., Zhou, X., 2018. Sens. Actuators, B 276, 421-428.
Li, Y., Ban, Y., Wang, R., Wang, Z., Li, Z., Fang, C., Yu, M., 2020. Chin. Chem. Lett. 31(2), 443-446.
Lin, Z., Liu, Z., Zhang, H., Su, X., 2015. Analyst 140(5), 1629-1636.
Lin, Z., Zhang, X., Liu, S., Zheng, L., Bu, Y., Deng, H., Chen, R., Peng, H., Lin, X., Chen, W., 2020. Anal. Chim. Acta. 1105, 162-168.
Liu, X., Freeman, R., Golub, E., Willner, I., 2011. Acs Nano 5(9), 7648-7655.
Liu, Z., Lin, Z., Liu, L., Su, X., 2015. Anal. Chim. Acta 876, 83-90.
Ma, X., Lin, S., Dang, Y., Dai, Y., Zhang, X., Xia, F., 2019. Anal. Bioanal. Chem. 411(25), 6645-6653.
Makarov, D.V., Loeb, S., Getzenberg, R.H., Partin, A.W., 2009. Annu. Rev. Med. 60, 139-151.
Minkin, C., 1982. Calcified Tissue Int. 34(1), 285-290.
Mitić, N., Smith, S.J., Neves, A., Guddat, L.W., Gahan, L.R., Schenk, G., 2006. Chem. Rev. 106(8), 3338-3363.
Na, W., Hu, T., Su, X., 2016a. Analyst 141(16), 4926-4932.
Na, W., Liu, Q., Sui, B., Hu, T., Su, X., 2016b. Talanta 161, 469-475.

Ohta, N., Robertson, A., 2006. Colorimetry: fundamentals and applications. John Wiley & Sons.
Pang, S., Liu, S., 2017. Anal. Methods 9(47), 6713-6718.
Pang, S., Liu, S., 2020. Anal. Chim. Acta. 1105, 155-161.
Passariello, C., Forleo, C., Micheli, V., Schippa, S., Leone, R., Mangani, S., Thaller, M.C., Rossolini, G.M., 2006. BBA-Proteins Proteomics 1764(1), 13-19.
Qian, Z., Chai, L., Zhou, Q., Huang, Y., Tang, C., Chen, J., Feng, H., 2015. Anal. Chem. 87(14), 7332-7339.
Qu, Z., Li, N., Na, W., Su, X., 2019. Talanta 192, 61-68.
Qu, Z., Na, W., Liu, X., Liu, H., Su, X., 2018. Anal. Chim. Acta 997, 52-59.
Schanda, J., 2007. Colorimetry: understanding the CIE system. John Wiley & Sons.
Sharma, A., Pandey, C.M., Matharu, Z., Soni, U., Sapra, S., Sumana, G., Pandey, M.K., Chatterjee, T., Malhotra, B.D., 2012. Anal. Chem. 84(7), 3082-3089.
Shi, F., Zhang, Y., Na, W., Zhang, X., Li, Y., Su, X., 2016. J. Mater. Chem. B 4(19), 3278-3285.
Siddiqua, A., Rehmat, M., Saeed, A., Amin, S., Naz, R., Sherazi, M., Khan, G.M., Saeed, A., 2008. Biol. Pharm. Bull. 31(5), 802-808.
Song, J., Wang, L., Qi, H., Qi, H., Zhang, C., 2019. Chin. Chem. Lett. 30(9), 1643-1646.
Song, W., Duan, W., Liu, Y., Ye, Z., Chen, Y., Chen, H., Qi, S., Wu, J., Liu, D., Xiao, L., 2017. Anal. Chem. 89(24), 13626-13633.
Strauss, V., Margraf, J.T., Dolle, C., Butz, B., Nacken, T.J., Walter, J., Bauer, W., Peukert, W., Spiecker, E., Clark, T., 2014. J. Am. Chem. Soc. 136(49), 17308-17316.
Sun, J., Yang, F., Yang, X., 2015. Nanoscale 7(39), 16372-16380.
Vääräniemi, J., Halleen, J.M., Kaarlonen, K., Ylipahkala, H., Alatalo, S.L., Andersson, G., Kaija, H., Vihko, P., Väänänen, H.K., 2004. J. Bone Miner. Res. 19(9), 1432-1440.
Valizadeh, M., Schenk, G., Nash, K., Oddie, G.W., Guddat, L.W., Hume, D.A., de Jersey, J., Burke Jr, T.R., Hamilton, S., 2004. Arch. Biochem. Biophys. 424(2), 154-162.
Veeramani, S., Lee, M., Lin, M., 2009. Trends Biochem. Sci. 34(6), 273-278.
Veeramani, S., Yuan, T., Chen, S., Lin, F., Petersen, J.E., Shaheduzzaman, S., Srivastava, S., MacDonald, R.G., Lin, M., 2005. Endocr-Relat. Cancer 12(4), 805-822.
Vincent, J.B., Crowder, M.W., Averill, B., 1992. Trends Biochem Sci. 17(3), 105-110.
Wang, J., Yan, Y., Yan, X., Hu, T., Tang, X., Su, X., 2016. Sens. Actuators, B 234, 470-477.
Wu, Y., Wei, P., Pengpumkiat, S., Schumacher, E.A., Remcho, V.T., 2015. Anal. Chem. 87(16), 8510-8516.
Xie, Y., Tan, Y., Liu, R., Zhao, R., Tan, C., Jiang, Y., 2012. ACS Appl. Mater. interfaces 4(8), 3784-3787.
Xu, M., Ma, R., Huang, C., Shi, G., Zhou, T., Deng, J., 2020. Anal. Chim. Acta 1096, 174-183.
Xu, Y., Li, B., Xiao, L., Ouyang, J., Sun, S., Pang, Y., 2014. Chem. Commun. 50(63), 8677-8680.
Yamauchi, Y., Ido, M., Maeda, H., 2005. J. Chromatogr. A 1066(1-2), 127-132.
Yamauchi, Y., Ido, M., Ohta, M., Maeda, H., 2004. Chem. Pharm. Bull 52(5), 552-555.
Yan, X., Xia, C., Chen, B., Li, Y.F., Gao, P.F., Huang, C.Z., 2019. Anal. Chem. 92(2), 2130-2135.
Yi, L., Li, H., Sun, L., Liu, L., Zhang, C., Xi, Z., 2009. Angew Chem, Int. Ed. 48(22), 4034-4037.
Zhang, J., Yuan, Y., Han, Z., Li, Y., van Zijl, P.C., Yang, X., Bulte, J.W., Liu, G., 2019a. Biosens. Bioelectron. 141, 111442.
Zhang, W., He, X., Li, W., Zhang, Y., 2012. Chem. Commun. 48(12), 1757-1759.
Zhang, X., Gao, N., Guan, Z., He, Y., 2016a. Chin. Chem. Let. 27(6), 964-968.
Zhang, X., Yuan, A., Mao, X., Chen, Q., Huang, Y., 2019b. Sens. Actuators, B 299, 126928.
Zhang, X., Zhu, Y., Li, X., Guo, X., Zhang, B., Jia, X., Dai, B., 2016b. Anal. Chim. Acta 944, 51-56.
Zhang, Y., Fu, Y., Zhu, D., Xu, J., He, Q., Cheng, J., 2016c. Chin. Chem. Lett. 27(8), 1429-1436.
Zhao, M., Feng, H., Han, J., Ao, H., Qian, Z., 2017. Anal. Chim. Acta 984, 202-210.

509 Zheng, M., Tan, H., Xie, Z., Zhang, L., Jing, X., Sun, Z., 2013. ACS Appl. Mater. Interfaces 5(3), 1078-1083.
510 Zheng, S., Gu, H., Yin, D., Zhang, J., Li, W., Fu, Y., 2020. Colloids Surf., A 589, 124444.
511 Zhong, J., Chen, X., Zhang, M., Xiao, C., Cai, L., Khan, W.A., Yu, K., Cui, J., He, L., 2020. Chin. Chem. Lett. 31(3),
512 769-773.
513 Zhu, Z., Lin, X., Wu, L., Zhao, C., Li, S., Liu, A., Lin, X., Lin, L., 2019. Microchim. Acta 186(8), 558.
514 Zhu, Z., Lin, X., Wu, L., Zhao, C., Zheng, Y., Liu, A., Lin, L., Lin, X., 2018. Sens. Actuators, B 274, 609-615.
515

Figures and Table

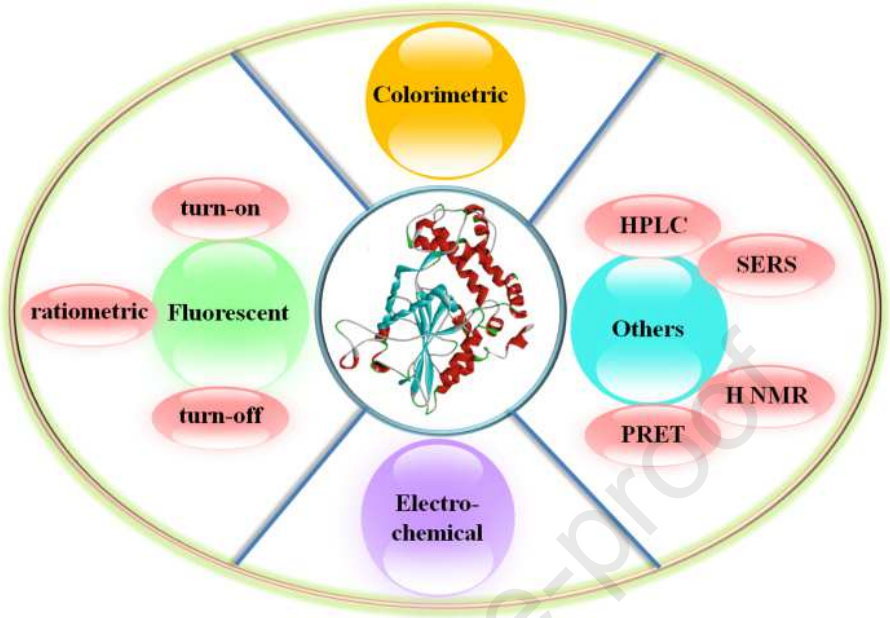

Fig. 1. Different strategies for detecting ACP.

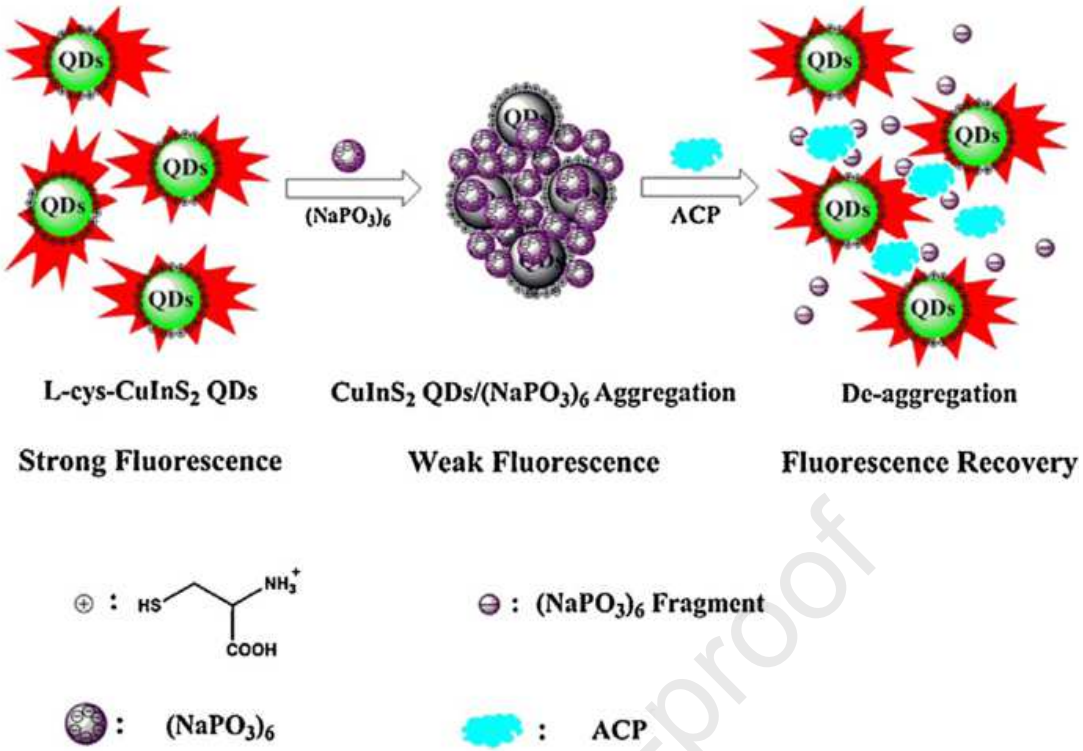

522

523

524 **Fig. 2**. Schematic diagram of L-cys-$CuInS_2$ QDs sensor for ACP sensing (Liu et al. 2015)
525 (Copyright, 2015; Elsevier).

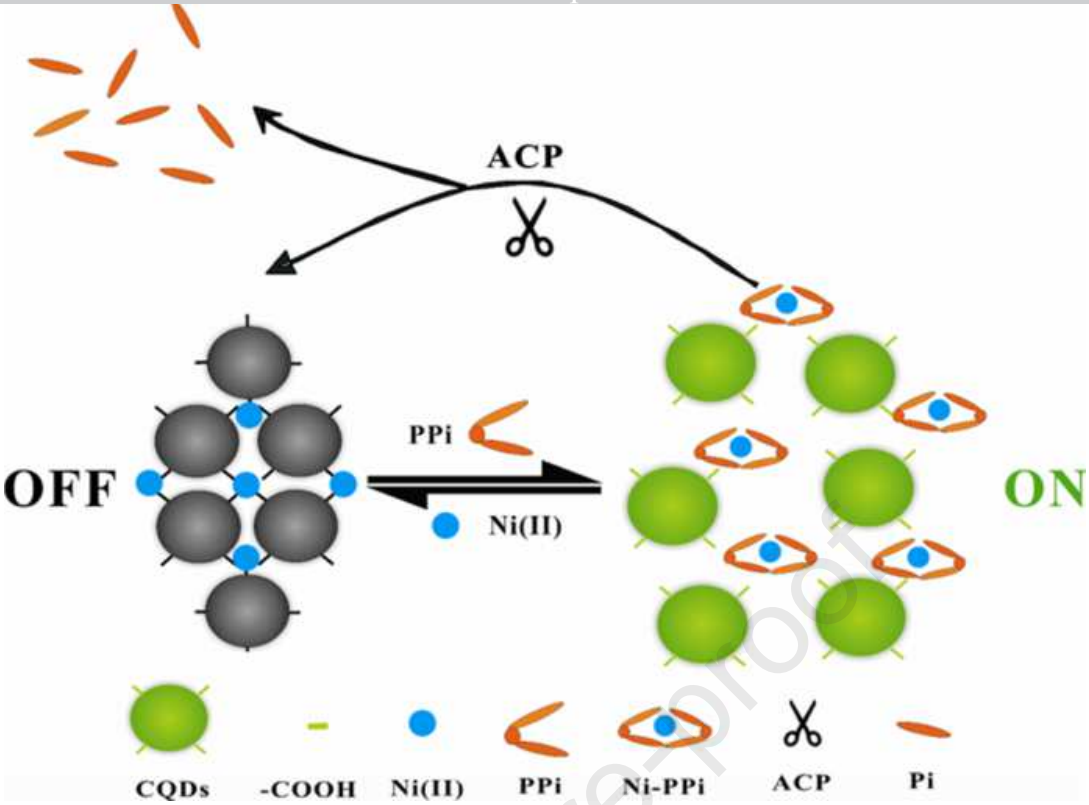

526

527

528 **Fig. 3**. Schematic diagram of reversible detection of ACP based on CQD sensor (Qian et al. 2015)

529 (Copyright, 2015; ACS Publications).

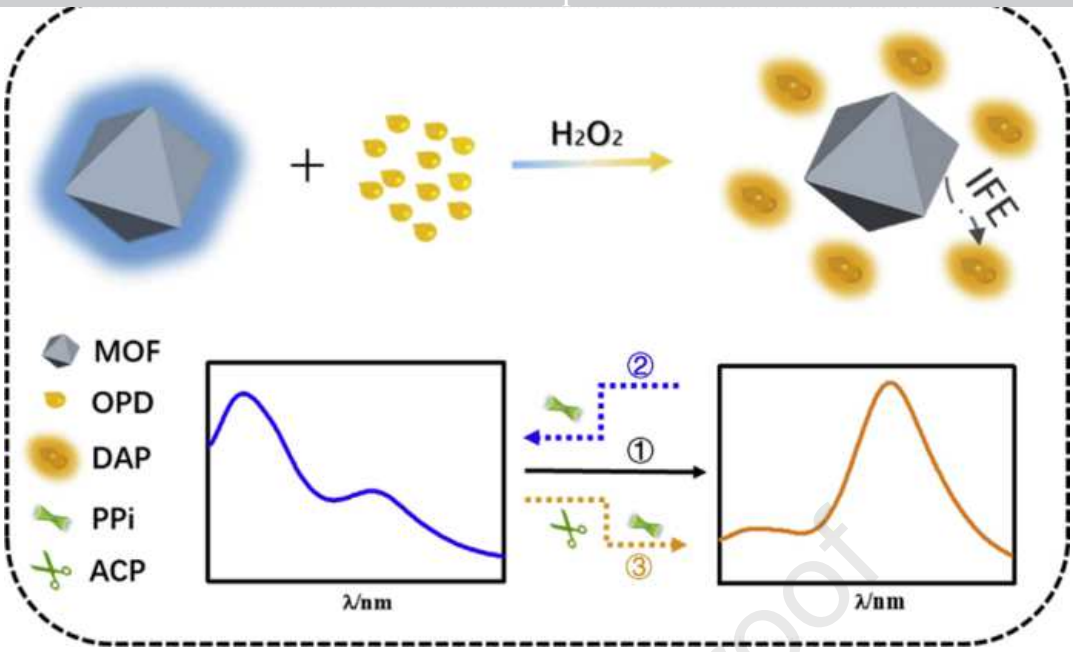

530

531

532 **Fig. 4**. Schematic diagram of NH_2-MIL-101 MOF sensor ratiometric detection of ACP (Li et al.
533 2019) (Copyright, 2019; Elsevier).

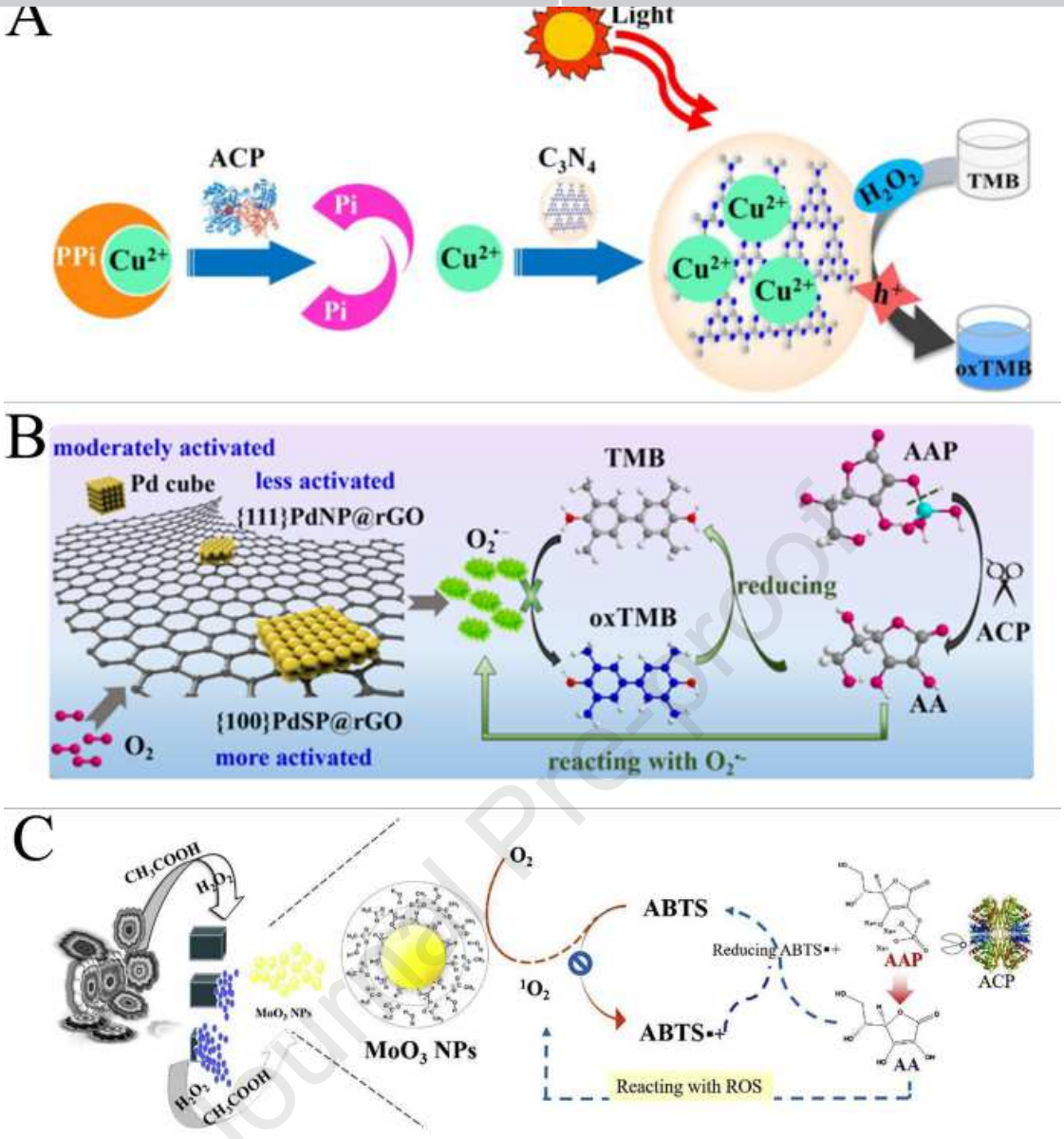

Fig. 5. Colorimetric detection of ACP based on (A) C_3N_4 nanosheets (Guo et al. 2019) (Copyright, 2019; ACS Publications); (B) oxidative mimic enzymes (Chen et al. 2019a) (Copyright, 2019; ACS Publications); (C) MoO_3 NPs peroxidase (Lin et al. 2020) (Copyright, 2020; Elsevier).

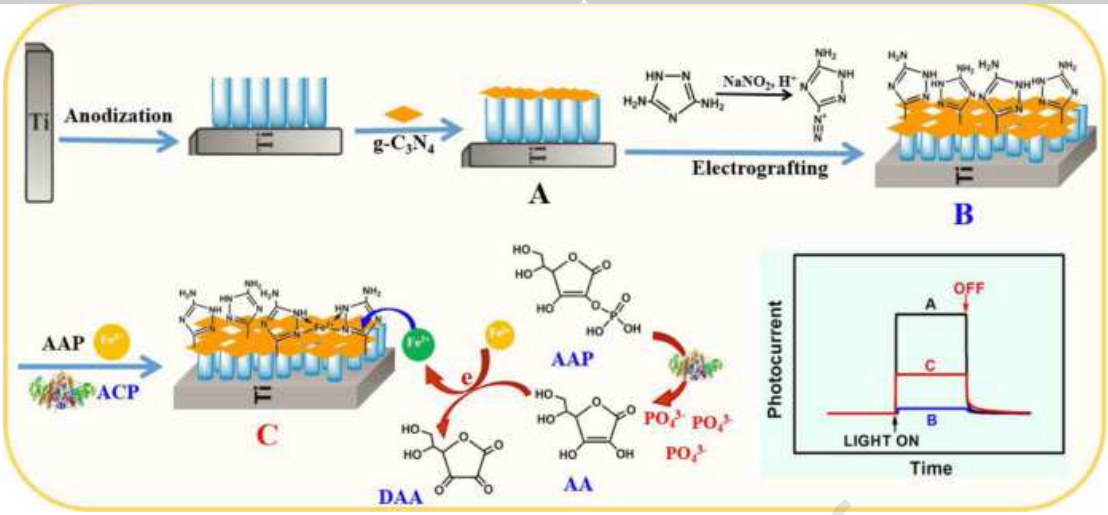

539

540

541 **Fig. 6**. Schematic diagram of TNA/g-C_3N_4/DAT sensor for detecting ACP (Huang et al. 2020)
542 (Copyright, 2020; Elsevier).

543 **Table 1.** Comparison of detection performance for ACP based on the different detection strategies.

detection strategy	material	intermedium	linear range	LOD	compatibility with tissues/ cellular	the total detection time	ref.
fluorescence turn-on	PPE4+	p-NPP	0-20 nM	0.17 nM	/	~180 min	(Xie et al. 2012)
	anionic water soluble polymer	p-NPP, Fe^{3+}	/	0.18 nM	/	>480 min	(Dwivedi and Iyer 2013)
	small molecular probe	$(NaPO_3)_6$	5-100 μunits/mL	/	/	~200 min	(Guo et al. 2013)
	squaraine dyes	$(NaPO_3)_6$	0-0.533 μM	4.9 nM	/	~180 min	(Xu et al. 2014)
	N-GQDs	AA2P, dopaquinone	0.04-0.7 U/L	0.014 U/L	/	40 min	(Qu et al. 2018)
	GQDs@GSH	AA2P	0.1-9 U/L	0.027 U/L	/	40 min	(Qu et al. 2019)
	N-CDs	AA2P	5-40 U/L	0.1 U/L	/	~120 min	(Zhu et al. 2018)
	CDs	Cu^{2+}, AA2P	100-2800 μM	60 μM	/	~60 min	(Ma et al. 2019)
	L-cys-$CuInS_2$ QDs	$(NaPO_3)_6$	75-1500 μU/L	9.02 μU/L	/	2 min	(Liu et al. 2015)
	Lys-Au/AgNCs	AA2P	100-12500 μg/L	53 μg/L	/	45 min	(Pang and Liu 2017)
	Au-NCs/MnO_2	AA2P	0.01-16 U/L	0.003 U/L	/	60 min	(Xu et al. 2020)
fluorescence turn-off	CQD	PPi, Ni^{2+}	18.2-1300 U/L	5.5 U/L	/	60 min	(Qian et al. 2015)
	GQDs	$Cr_2O_7^{2-}$, AA2P	0.02-3 U/L	8.9 mU/L	/	~120 min	(Shi et al. 2016)
	GQDs	PDDA, $(NaPO_3)_6$	30-420 μU/L	12 μU/L	/	~40 min	(Na et al. 2016a)
	CDs	dopamine	1-60 U/L	0.45 U/L	/	100 min	(Chen et al. 2019c)
	AuNCs@GSH/MUA	PPi, Fe^{3+}	1-30 nM	1 nM	/	30 min	(Sun et al. 2015)
	CuNCs	p-NPP	3.8-22.8 U/L	1.3 U/L	/	16 min	(Huang et al. 2016)
	CuNCs	PPi, Fe^{3+}	2.2-45.5 U/L	0.8 U/L	/	12 min	(Zhao et al. 2017)
	$CuInS_2$ QDs	Cu^{2+}, ATP	6.4-192 μU/L	3.1 μU/L	PC-3M cells biocompatible	~30 min	(Lin et al. 2015)
	CdTe QDs	ATP	1.0-50 mU/L	0.45 mU/L	/	~40 min	(Wang et al. 2016)
ratiometric fluorescence	GQDs-NR	lecithin/β-CD complex	0-1500 mU/L	28 mU/L	PC-3 M cells biocompatible	90 min	(Na et al. 2016b)
	NH_2-MIL-101 MOF	PPi	0.01-30 U/L	0.005 U/L	/	60 min	(Li et al. 2019)
	N-CDs	$(NaPO_3)_6$	1-50 U/L	0.43 U/L	HepG2 cells biocompatible	120 min	(Zhu et al. 2019)
	GN-CDs	PPi, Fe^{3+}	0.08-6.75	0.01 mg/L	/	60 min	(Pang and Liu

			mg/L				2020)
colorimetric	$Cu(BCDS)_2^{2-}$	AA2P	0-220 U/L	3.16 U/L	/	30 min	(Hu et al. 2016)
	Ch-PtNPs	AA2P, TMB	0.25-2.5 U/L	0.016 U/L	/	35 min	(Deng et al. 2017)
	C_3N_4	Cu^{2+}-PPi, TMB	0.05-40 U/L	8.8 mU/L	/	45 min	(Guo et al. 2019)
	AuPd nanozymes	AA2P, TMB	1-14 U/L	0.53 U/L	/	40 min	(Zheng et al. 2020)
	BP-PEG-AuNPs	/	1 pg/L-1 g/L	0.3 pg/L	/	10 min	(Haddada et al. 2017)
	Pd/Pt NWs	AA2P, TMB	0.17-2.67 U/L	0.06 U/L	/	50 min	(Jin et al. 2019)
	Co/Mn oxide nano- composite	AA2P, TMB	0.02-1.0 U/L	8.2 mU/L	/	38 min	(Zhang et al. 2019b)
	Pd nanoplates enclosed by {100}- facets [{100}PdSP @rGO]	AA2P, TMB	0.01-6.0 U/L	8.3 mU/L	/	35 min	(Chen et al. 2019a)
	MoO_3 NPs	AA2P, ABTS	0.09-7.3 U/L	0.011 U/L	/	60 min	(Lin et al. 2020)
electro-chemical	poly(vinyl chloride) matrix membrane	p-NPP	50-3000 IU/L	0.03-0.05 enzyme IU/L	/	<10 min	(Hassan et al. 2009)
	poly (vinyl chloride) matrix membrane	1-NAP	0.01-4.3 IU/L	0.01 enzyme IU/L	/	<10 min	(Kamel et al. 2014)
	Cu (II) TC Pc-PAA	2-naphthyl phosphate	0.5-20 nM	0.5 nM	/	10 min	(Fredj et al. 2019)
	TNA/g-C_3N_4/DAT	Fe^{3+}, AA2P	0.05-100 U/L	0.016 U/L	/	15 min	(Huang et al. 2020)
	not specified	p-NPP disodium salt	/	/	/	>30 min	(Yamauchi et al. 2004)
HPLC	mightysil RP-18 GP and inertsil WP300 C18	p-NPP	/	/	/	>30 min	(Yamauchi et al. 2005)
SERS	MIPs	MPBA-modified AuNPs	18.2 pM-1.82 μM	18.2 pM	/	~85 min	(Li et al. 2018)
H NMR	/	p-NPP	5-50 U/L	5 U/L	/	>60 min	(Zhang et al. 2019a)
PREF	UGPs	AA2P	0.1-5.0 U/L	0.076 U/L	/	35 min	(Yan et al. 2019)

544

Highlights

- The status of ACP detection around fluorescence, colorimetric, and electrochemical were reviewed.
- The types and advantages/disadvantages of ACP detection methods were summarized and compared.
- The prospects and trends of ACP detection were proposed.

Declaration of interests

x The authors declare that they have no known competing financial interests or personal relationships that could have appeared to influence the work reported in this paper.

☐The authors declare the following financial interests/personal relationships which may be considered as potential competing interests: